

Article

Rare-Earth-Ion (RE³⁺)-Doped Aluminum and Lanthanum Borates for Mobile-Phone-Interrogated Luminescent Markers

Katya Hristova ¹, Irena P. Kostova ¹ , Tinko A. Eftimov ^{2,3,*} , Daniel Brabant ² and Samia Fouzar ²

¹ Department of Chemical Technology, Faculty of Chemistry, Plovdiv University “Paisii Hilendarski” 24 Tsar Asen Str., 4000 Plovdiv, Bulgaria; kathhristova@gmail.com (K.H.); irena_k87@abv.bg (I.P.K.)

² Photonics Research Center, Université du Québec en Outaouais, rue 101 St-Jean Bosco, Gatineau, QC J8X 3G5, Canada; dbrabant426@gmail.com (D.B.); sfouzar@cdta.dz (S.F.)

³ Central Laboratory of Applied Physics, Bulgarian Academy of Sciences, 61 Sanct Peterburg Blvd., 4000 Plovdiv, Bulgaria

* Correspondence: tinko.eftimov@uqo.ca

Abstract: In this paper, we present the synthesis and luminescent spectra of rare-earth (RE)-doped aluminum and lanthanum borates intended to serve as narrow excitation–emission band fluorescent markers. We perform a detailed 3D excitation–emission matrix (EEM) analysis of their spectra, compare the measurements from both standard and mobile phone spectrometers, and outline the basic differences and advantages of each method. While smartphones have a different and non-uniform spectral response compared to standard spectrometers, it is shown that they offer a number of advantages such as contactless interrogation, efficient suppression of the UV excitation light, and simultaneous spectral analysis of spatially arranged arrays of fluorescent markers. The basic emission peaks have been observed and their corresponding electronic transitions identified. The obtained results show that the rare-earth-doped La and Al borates feature excitation–emission bandwidths as low 15 nm/12 nm, which makes them particularly appropriate for use as luminescent markers with UV LED excitation and smartphone interrogation.

Keywords: rare earth; aluminum borates; lanthanum borates; smartphone interrogation; excitation–emission matrices; fluorescence; luminescent markers



Citation: Hristova, K.; Kostova, I.P.; Eftimov, T.A.; Brabant, D.; Fouzar, S. Rare-Earth-Ion (RE³⁺)-Doped Aluminum and Lanthanum Borates for Mobile-Phone-Interrogated Luminescent Markers. *Photonics* **2024**, *11*, 434. <https://doi.org/10.3390/photronics11050434>

Received: 23 March 2024

Revised: 21 April 2024

Accepted: 29 April 2024

Published: 6 May 2024



Copyright: © 2024 by the authors. Licensee MDPI, Basel, Switzerland. This article is an open access article distributed under the terms and conditions of the Creative Commons Attribution (CC BY) license (<https://creativecommons.org/licenses/by/4.0/>).

1. Introduction

In recent years, inorganic borate materials synthesized by the solid-state method have attracted considerable attention due to their promising chemical and physical properties and applications such as flat panel displays, white-light-emitting diodes (WLEDs), solar cells, thermoluminescent dosimeters, plasma displays, etc. [1]. In these applications, rare earth (RE) compounds are highly valued due to their unique electron configurations. Key RE³⁺ elements such as La, Ce, Sm, Eu, Gd, Tb, and Dy primarily exist in the +3 valence state, characterized by up to 14 electrons in the 4f shell. These ions can also occur in +4 and +2 valence states when their f shells are partially filled. In these materials, luminescence occurs through processes including absorption, excitation, energy transfer, and emission, triggered by electron transitions between energy orbitals. In these systems, the host material plays an important role. It acts as a passive matrix defining the spatial positions of dopant ions, termed activators, and as an active participant that influences the spectroscopic properties of these activators [2]. For instance, terbium (Tb³⁺) and cerium (Ce³⁺) ions, with their 4f-5d excited states, demonstrate efficient luminescence when incorporated into lanthanum and aluminum compounds [3].

Borate compounds can feature a three- or four-fold coordination of borate atoms, which perform as excellent hosts for luminescent materials due to their structural diversity [4]. Rare earth elements like Sm, Tb, Eu, Ce, Gd, and Dy, when doped into lanthanum and aluminum borates, can enhance luminescence properties. For example, Eu³⁺ shows strong

red/orange luminescence, while Tb³⁺ emits in the green spectrum [5]. Various synthesis methods such as the high-temperature solid-state reaction, sol–gel, hydrothermal synthesis, and solution combustion are employed, with the solid-state reaction noted for its simplicity, high yield, and environmentally friendly profile. The applications of Eu-doped La and Al borates are diverse due to their unique excitation–emission spectra [6,7]. These include uses in anti-counterfeiting [8,9] and potential applications in plasma displays [10]. In all of the above and in other applications, it is of crucial importance to be able to detect, identify, and track such luminescent markers remotely using worldwide available smartphones [11–16], which are more affordable than professional spectrometers and are compatible with Internet of Things technology, thus allowing intelligent sensing networks to be developed.

In the present work, we synthesized a series of luminescent lanthanum and aluminum borate samples doped with various rare earth elements and their combinations in order to obtain a unique coding for various applications. We measured the 3D excitation–emission spectra of the samples with a standard optical fiber spectrophotometer and with a smartphone in combination with a transmission diffraction grating, referred to hereafter as a smartphone or mobile phone spectrometer.

2. Synthesis of the Eu³⁺-Doped Borates

2.1. Materials

The following reagents of analytical grade purity were used for the synthesis of luminescent materials: La₂O₃ (lanthanum (III) oxide, 99.9%) and Al₂O₃ (aluminum oxide for chromatographic purposes 99%), purchased from Alfa Aesar, H₃BO₃ (boric acid, 99%, index # 005-007022-2), Eu₂O₃ (europium (III) oxide, 99.99% (trace metal basis), Acros, CAS: 1308-96-9), Sm₂O₃, Dy₂O₃, Gd₂O₃, Ce(SO₄)₂ × 4 H₂O, and TbF₃.

2.2. Synthesis of LaBO₃: RE and AlBO₃: RE Phosphors

In our experiments, LaBO₃: RE and AlBO₃: RE (Re—Eu₂O₃, Sm₂O₃, Dy₂O₃, Gd₂O₃, Ce(SO₄)₂ × 4 H₂O, and TbF₃) phosphors were synthesized by the solid-state method. The solid-state synthesis was carried out in a muffle furnace LM 312.07 with a G400 controller and a temperature range of 0–1200 °C. The raw materials La₂O₃, Al₂O₃, and an excess of H₃BO₃ –45% were used according to the stoichiometric formulas shown in Equations (1) and (2):



All of these samples were doped with a mol % varying from 1 to 3 mol % of each rare earth compound and a combination of them as shown in Table 1. For the synthesis, reagents were weighed, mixed, and well-homogenized. The prepared mixtures were placed in porcelain crucibles. In the muffle furnace, the samples were heated in a controlled manner, where slow heating at a rate of ~15 °C/min was applied to set the temperature to 1050 °C for samples A3–A11, maintained for 6 h, and 1000 °C for samples B1–B12, A1, and A2, again for 6 h, and after that they were left in the furnace and cooled slowly for 16 h. After cooling, the samples of LaBO₃: RE were a fine white powder and the AlBO₃: RE samples were in a crystalline-like form. Furthermore, they could be crushed into a fine powder. In order to compare the host-to-activator efficiency in LaBO₃/AlBO₃, we synthesized LaBO₃/AlBO₃ doped with different lanthanide ions and combinations of them (Eu³⁺, Sm³⁺, Dy³⁺, Gd³⁺, Ce⁴⁺, Eu³⁺/Tb³⁺, Eu³⁺/Ce⁴⁺, Eu³⁺/Gd³⁺, and Eu³⁺/Gd³⁺/Tb³⁺). The combination of rare earth (RE) ions in LaBO₃ and AlBO₃ matrices improves their optical properties, making them suitable for various applications and easy to check using smartphone equipment. Cerium ions were employed as a co-doping agent because they are capable of transferring energy to other RE ions such as europium (Eu³⁺), which significantly enhances their luminescent properties. In samples A8 and B8, for example, the emission of Eu³⁺ ions was greatly enhanced by the energy transfer from cerium to europium ions.

When combined with Eu^{3+} , gadolinium performs as a sensitizing agent, improving the luminescence efficiency of europium ions. This is due to the half-filled orbital of gadolinium ions. Therefore, the combination of gadolinium and europium ions can largely enhance the luminescent properties of borate materials.

Table 1. List and notation of the synthesized samples.

$\text{La}_2\text{O}_3 + \text{H}_3\text{BO}_3$ Sample Notation	RE	Mol % of REs	$\text{Al}_2\text{O}_3 + \text{H}_3\text{BO}_3$ Sample Notation	RE	Mol % of REs
A1	Eu_2O_3	2	B1	Eu_2O_3	2
A2	Sm_2O_3	2	B2	Sm_2O_3	2
A3	Dy_2O_3	2	B3	-	-
A4	-	-	B4	TbF_3	2
A5	Gd_2O_3	2	B5	-	-
A6	$\text{Ce}(\text{SO}_4)_2 \times 4 \text{H}_2\text{O}$	2	B6	$\text{Ce}(\text{SO}_4)_2 \times 4 \text{H}_2\text{O}$	2
A7	$\text{Eu}_2\text{O}_3 + \text{TbF}_3$	2/1	B7	$\text{Eu}_2\text{O}_3 + \text{TbF}_3$	2/1
A8	$\text{Eu}_2\text{O}_3 + \text{Ce}(\text{SO}_4)_2 \times 4 \text{H}_2\text{O}$	2/1	B8	$\text{Eu}_2\text{O}_3 + \text{Ce}(\text{SO}_4)_2 \times 4 \text{H}_2\text{O}$	2/1
A9	-	-	B9	$\text{Eu}_2\text{O}_3 + \text{Dy}_2\text{O}_3$	2/1
A10	$\text{Eu}_2\text{O}_3 + \text{Gd}_2\text{O}_3$	2/1	B10	$\text{Eu}_2\text{O}_3 + \text{Gd}_2\text{O}_3$	2/1
A11	$\text{Eu}_2\text{O}_3 + \text{Gd}_2\text{O}_3 + \text{TbF}_3$	3/2/1	B11	-	-
A12	-	-	B12	$\text{Eu}_2\text{O}_3 + \text{Dy}_2\text{O}_3 + \text{TbF}_3$	3/2/1

3. Fluorescence Spectra

3.1. Experimental Setup

The experimental setup used for the measurement of the fluorescence spectra with both a standard spectrometer and mobile phone spectrometer is shown in Figure 1a,b. A laser-driven light source (Energetiq, Wilmington, MA, USA) generates white light in the 190–2500 nm range, which is coupled to an Ocean Optics, Orlando, FL, USA (QE 65000) monochromator via a 1 mm-diameter large core fiber. The optical fiber spectrometer covers a range from 200 to 900 nm. A 1 mm hole is drilled in a plastic platform, in which are installed 600 μm core lead-in and lead-out fibers at 90° with respect to each other. The lead-in fiber excites the sample, and the lead-out fiber couples the fluorescence and scattered light to the standard Ocean Optics (OO) spectrometer as shown in Figure 1a. The fluorescent sample is observed by the smartphone camera from a distance of about 15 cm, at which distance the smartphone can focus on the fluorescent sample. The mobile phone used is a Samsung Galaxy A51 (2400 × 1080 pixels).

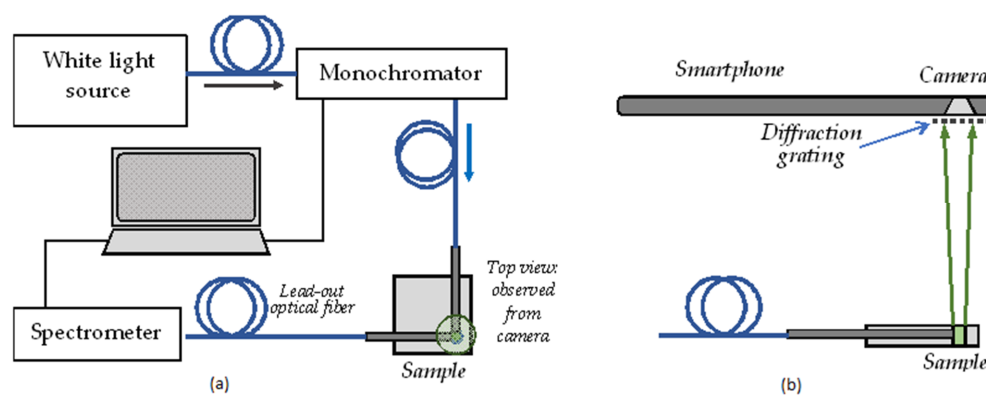


Figure 1. Experimental setup: (a) basic arrangements for the measurement of the 3D excitation–emission spectra of the samples using a standard optical fiber spectrometer; (b) side view of the arrangement from (a) with a smartphone camera equipped with a sheet transmission diffraction grating (1000 L/mm) to observe the spectrum.

3.2. Measurements with a Spectrometer and a Monochromator

3.2.1. Excitation–Emission Spectra

The standard procedure is to scan the excitation wavelength λ' within a certain range and measure the luminescence spectrum for each excitation wavelength, which allows us plot 3D excitation–emission spectra, the topographic views of which are shown for sample A3 and B4 in Figure 2. It is well known that lanthanide ions have very low absorption coefficients ($\epsilon \leq 1 \text{ M}^{-1} \text{ cm}^{-1}$) [15]. To increase light emission, the lanthanide ion can be doped into suitable matrices.

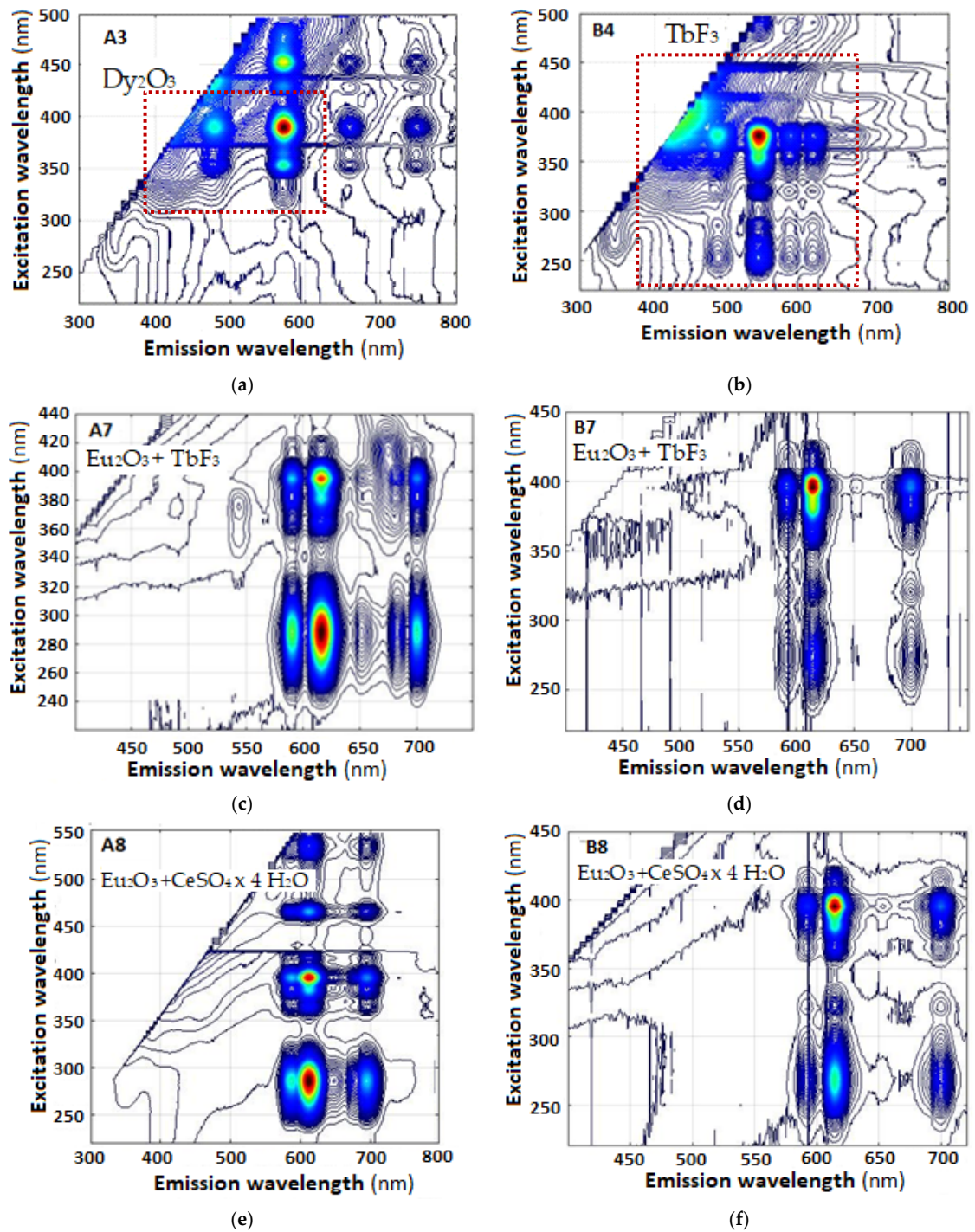


Figure 2. Cont.

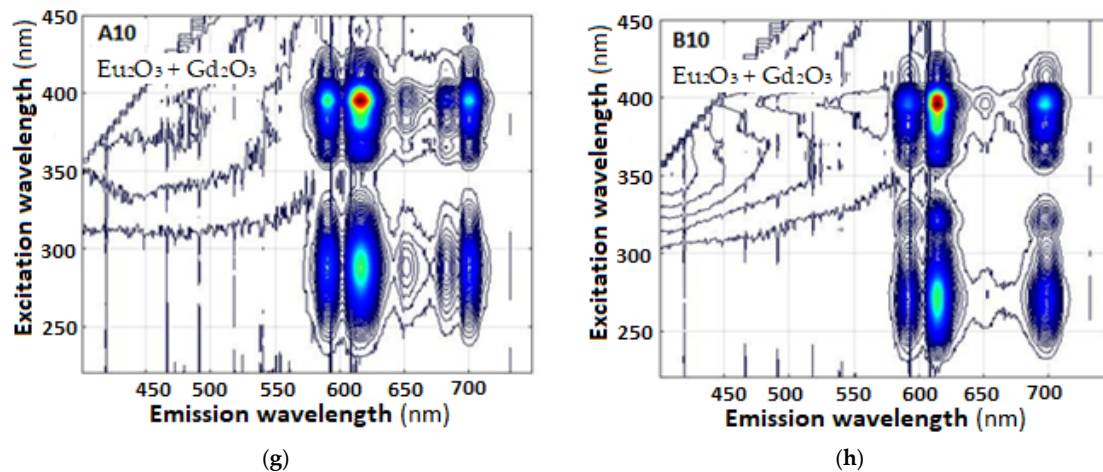


Figure 2. Topographic views of the excitation–emission fluorescence spectra measured by an Ocean Optics spectrometer of synthesized samples from the A ($\text{La}_2\text{O}_3 + \text{H}_3\text{BO}_3$) and B ($\text{Al}_2\text{O}_3 + \text{H}_3\text{BO}_3$) groups: (a) A3—(Dy_2O_3); (b) B4—(TbF_3); (c) A7 and (d) B7—($\text{Eu}_2\text{O}_3 + \text{TbF}_3$); (e) A8 and (f) B8—($\text{Eu}_2\text{O}_3 + \text{Ce}(\text{SO}_4)_2 \times 4 \text{H}_2\text{O}$); (g) A10 and (h) B10—($\text{Eu}_2\text{O}_3 + \text{Gd}_2\text{O}_3$). The red rectangles show the wavelength ranges within which the spectra were measured with the smartphone.

The lowest excited energy level ($^4\text{F}_{9/2}$) of the Dy^{3+} ion (478 nm) (A3) is similar to that ($^5\text{D}_4$) of the Tb^{3+} ion (490 nm) (B4), and dysprosium (III) complexes exhibit the characteristic $^4\text{F}_{9/2} \rightarrow ^6\text{H}_{13/2}$ and $^4\text{F}_{9/2} \rightarrow ^6\text{H}_{15/2}$ transitions leading to blue (around 478 nm) and the most intensive emission, yellow (around 574 nm), respectively, as shown in Figure 2a [16]. The emission spectra in sample B4 are in two luminescence bands—a weak emission at around 481 nm in blue region corresponding to the transitions $^5\text{D}_4 \rightarrow ^7\text{F}_6$ obeys the magnetic dipole transition selection rule of $\Delta J = \pm 1$ [17,18] and a very strong one centered at 543 nm, relevant to transition $^5\text{D}_4 \rightarrow ^7\text{F}_5$, in strong green region, respectively, as shown in Figure 2b.

When a sample is doped with Tb^{3+} and Eu^{3+} , additional luminescence bands are observed as seen in Figure 2c for A7. The detailed spectroscopic analysis shows that these bands correspond to the $^5\text{D}_0 \rightarrow ^7\text{F}_J$ ($J = 1 \div 4$) transitions of Eu^{3+} , specifically $^5\text{D}_0 \rightarrow ^7\text{F}_2$ (Eu^{3+}) and $^5\text{D}_4 \rightarrow ^7\text{F}_5$ (Tb^{3+}) [19]. Their relative band intensities depend strongly on the concentrations of Tb^{3+} and Eu^{3+} in the materials. Figure 2c shows luminescent bands located in the spectral range of 590–620 nm, where both the $^5\text{D}_4 \rightarrow ^7\text{F}_5$ transitions of Tb^{3+} and $^5\text{D}_0 \rightarrow ^7\text{F}_J$ ($J = 0, 1$) of Eu^{3+} exist, suggesting a $\text{Tb}^{3+} \rightarrow \text{Eu}^{3+}$ energy transfer process. The reverse process, i.e., $\text{Eu}^{3+} \rightarrow \text{Tb}^{3+}$, is not observed [20].

The emission of the cerium ion originates from the allowed transition of $4f_0 5d_1 \rightarrow 4f_1 5d_0$. It is noted that $d \leftrightarrow f$ transitions depend strongly on the ligand field, allowing the emission peak of the cerium ion to range from ultraviolet to visible wavelengths [21].

The excitation spectrum of sample A8 in Figure 2e exhibits a broad band with two intense peaks at around 620 nm when excited by different sources: at 290 nm, corresponding to the $2\text{F}_5/2 \rightarrow 5d_2$ transition, and at 390 nm. In comparison, sample B8 (Figure 2f) shows a band with one intense peak at around 620 nm when excited by a source wavelength of 390 nm.

For a europium-to-cerium ion ratio of 2:1, the emission intensities of Eu^{3+} are higher compared to those of the cerium ion, which is indicative of efficient energy transfer from the cerium ion to Eu^{3+} . The dominant emission line observed is the $^5\text{D}_0 \rightarrow ^7\text{F}_2$ transition at around 620 nm, with all other lines being very weak in intensity, suggesting a low probability of the presence of orange and green Eu^{3+} emission lines [22].

Under the charge transfer excitation wavelength, the cerium ion emission band is observed along with the Eu excitation lines. The cerium emission band extends to cover all the Eu excitation lines, indicating that Ce transfers some of its energy to the Eu ion. Increasing the Eu concentration enhances the intensity of Eu lines while decreasing the intensity of the Ce emission band. Thus, the energy transfer process is incomplete, likely

involving both radiative and non-radiative energy transfers in samples A8 and B8, with Ce acting as the sensitizer and the Eu ion as the activator in the host matrix [23].

After direct Eu^{3+} excitation at 394 nm, the non-radiative relaxation (NR) takes Eu^{3+} down to the $^5\text{D}_0$ luminescence level. The excitation peaks of Gd^{3+} are found at around 275 nm, corresponding to the energy transfer of $^8\text{S}_{7/2} \rightarrow ^6\text{I}_{7/2}$ for samples with aluminum and lanthanum borate, as shown in Figure 3a,b. At this state, a few Gd^{3+} ions emit photons while most of the Gd^{3+} transfers energy to the Eu^{3+} ion. The Eu^{3+} acceptors then drop their energy to the $^5\text{D}_0$ level for luminescence. In the case of charge transfer excitation at 260 nm, Eu^{3+} receives an electron from O_2 , converting it to Eu^{2+} at the ground state with higher vibrational levels, as shown in Figure 2h. Some Eu^{2+} ions transfer energy to Gd^{3+} , while the remaining Eu^{2+} thermalizes non-radiative relaxation to the lowest vibrational level of the ground state before transferring energy to Eu^{3+} . Then, the Eu^{3+} and Gd^{3+} ions emit photons, and most of the Gd^{3+} also transfers energy to Eu^{3+} . Since the excitation energy at 260 nm is close to the $^6\text{D}_{5/2}$ level of Gd^{3+} , there exists the probability that light at 260 nm could also excite the Gd^{3+} ions. From these mechanisms, the $\text{Gd}^{3+} \rightarrow \text{Eu}^{3+}$ energy transfer is a key process [24]. The most intensive peak is at 613 nm for both of samples (A10 and B10), which is due to an electronic transition of Eu^{3+} ($^5\text{D}_0 \rightarrow ^7\text{F}_2$).

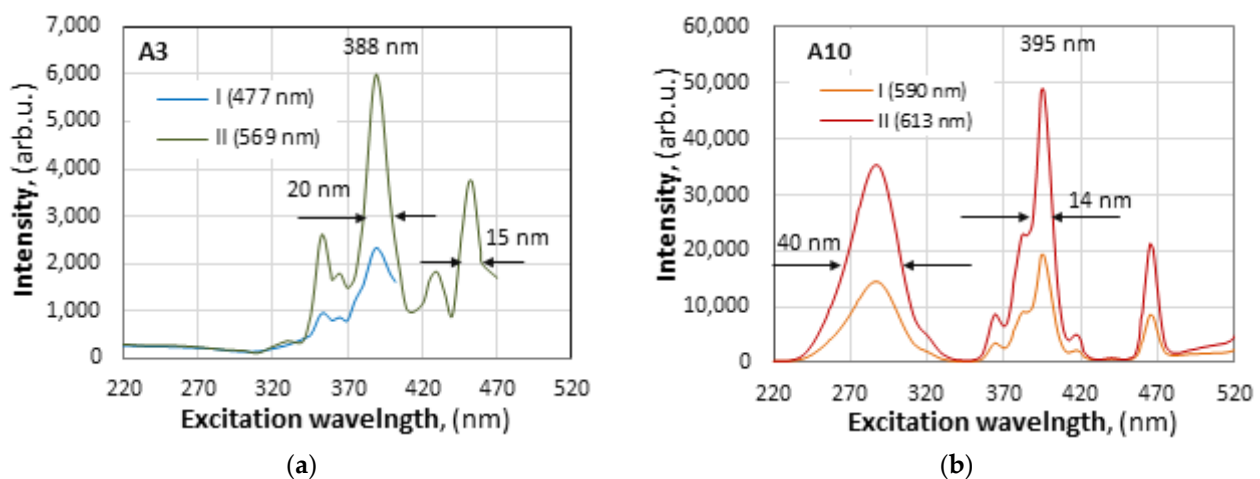


Figure 3. Excitation efficiency spectra and bandwidths of samples: (a) A3 and (b) A10.

3.2.2. Excitation–Emission Bandwidths

The 3D plots allow us to identify the excitation wavelength λ'_{max} of maximum intensity observed at the emission wavelength λ_{max} . In Figure 3, we observe these spectra as narrow excitation–emission maxima.

More details on the excitation spectra, the energy diagrams, and the FTIR spectra of these samples are presented in ref. [25].

4. Measurements with a Smartphone and a Monochromator

To measure the 3D excitation–emission spectra using a smartphone, we make use of the optical scheme in Figure 1b. The scheme allows two options: without a lens and with an additional lens. We first take a measurement without and then with a lens and make a comparison.

4.1. Smartphone Spectral Characteristics

The use of a smartphone to analyze spectral responses of luminescent materials usually performed with standard spectrometers requires a comparison of their spectral responses. The spectral response of a spectrometer is determined by the spectral sensitivity curve of the photodiode array and the spectral efficiency of the diffraction grating. The spectral response of the smartphone is determined by the transmission spectra of the RGB pixels, an example of which for Android smartphones is presented [15] in Figure 4. Figure 5a shows

the experimental setup that allows for the simultaneous measurement of the responses of the spectrometer and smartphone (Samsung A51) with a 1000 l/mm transmission grating. White light with power P is emitted into a monochromator whose output is varied from 390 nm to 700 nm, and further emitted into a 50%/50% optical fiber splitter. One signal $I_{OO}(\lambda)$ is observed by means of the spectrometer (OO—Ocean Optics) and the other $I_{MP}(\lambda)$ by the mobile phone. We then calculate the ratio as follows:

$$r(\lambda, P) = \frac{I_{MP}(\lambda, P)}{I_{OO}(\lambda, P)} \text{ for } P = \text{const} \tag{3}$$

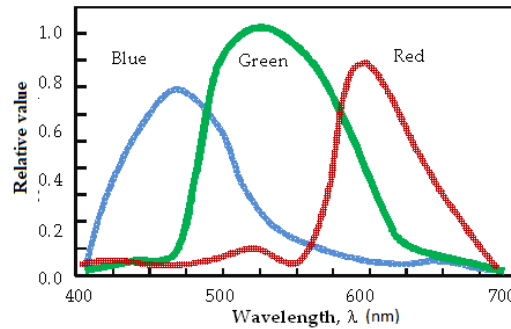


Figure 4. The transmission spectra of the R, G, and B pixels of an Android smartphone [15].

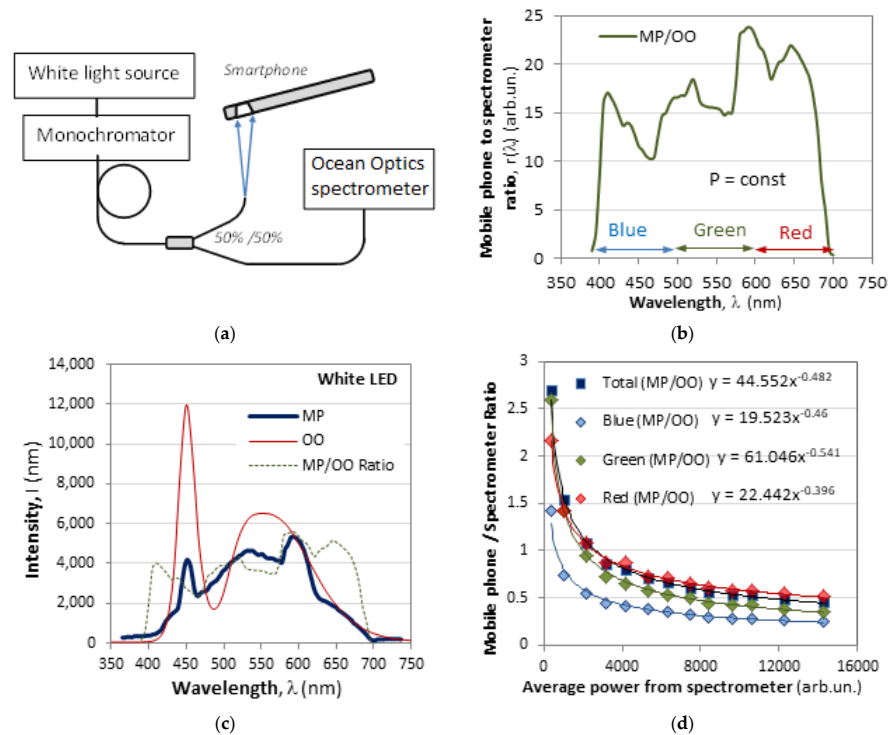


Figure 5. Spectrometer vs. smartphone comparison: (a) an auxiliary experimental setup to compare spectrometer and smartphone responses; (b) the spectral dependence of the ratio $r(\lambda)$ between the signal from the mobile phone to that of the spectrometer for a given signal level $P(\lambda)$; (c) a white LED spectrum as measured by a spectrometer (OO) and a smartphone (MP); (d) the $r(P)$ dependence for each of the R, G, and B spectral ranges.

The wavelength dependence $r(\lambda)$ is shown in Figure 5b. It is quite uneven and exhibits some minima at the boundary of the RGB spectral ranges, corresponding to the intersection of the RGB transmission spectra in Figure 4.

To test if the smartphone linearly responds to the level of the signal, we replace the constant-power, laser-driven white light source with a white LED whose output power can be varied. We measure the spectra with both the spectrometer and mobile phone, and from each spectrum we calculate the power in the blue, green, and red spectral ranges indicated in Figure 5b. In Figure 5c, we show the white LED spectrum as measured by the spectrometer (thin red line) and the mobile phone (thick blue line). The thin dotted line is a multiple of the ratio in Figure 5b and shows that the distortions of the LED spectrum as measured by the spectrometer are caused by the specific RGB transmission filters of the smartphone. Figure 5d presents the ratio $r(P)$ as a function of the optical power of the LED source for the three spectral ranges of blue, green, and red, and as a function of the total power as measured by the spectrometer. We see that as the optical power of the detected light increases, the intensity detected by the smartphone compared to that measured by the spectrometer decreases with the signal level, i.e., the smartphone signal tends to reach saturation following a power law of the type

$$r(P) = R \cdot P^{-p} \tag{4}$$

where the coefficient R and the power p depend on the pixel color. The effect is stronger for the blue part of the spectrum and the weakest for the red part, which is evident from Figure 5c where we see that the blue peak appears much weaker with the smartphone than the green and red components. The smartphone thus distorts the shape of the detected spectrum and is signal-power-dependent. These distortions depend on the particular mobile phone model and create the necessity for calibration [16].

4.2. Measurements without a Lens

A low-cost transmission sheet grating with 1000 lines/mm is placed in front of the smartphone’s camera. The spectra measured by the smartphone are taken simultaneously with those measured by the spectrometer.

Figure 6 shows stacks of photos of observed spectra taken by a smartphone with excitation varying from 220 nm to 420 nm. All images are processed using a custom-made software that is written in Python and makes use of the Numpy, Panda, Matplotlib, and OpenCV frameworks. The total intensity of the vertical column of activated pixels is presented as a function of the horizontal pixel position. For the purposes of wavelength calibration, the position of the zero-th order is considered $\lambda_0 = 0$ nm. Excitation wavelengths above 400 nm appear on the screen of the smartphone as shown in Figure 6a,b and can be used to plot the dependence $\lambda(N)$, where N is the number of the pixel corresponding to the wavelength λ . The dependence is linear as seen in Figure 6c, and we can write it in the following form:

$$\lambda(N) = \Lambda_0 + S_N N \tag{5}$$

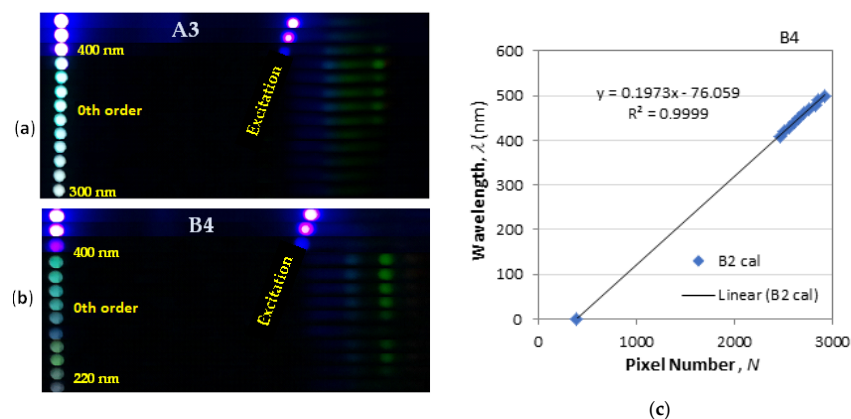


Figure 6. Stacked images of the spectra of samples (a) A3 and (b) B4 measured by the smartphone at excitations from 220 nm to 420 nm; (c) the $\lambda(N)$ plot for B4.

The factor $D = 1/S_N$ is the dispersion of the smartphone spectrometer and depends on the magnification of the camera. For the spectrum images of B4 (Figure 6b), $S_N = 0.1973 \text{ nm/pxl}$, so the dispersion is $D = 5.0684 \text{ pixels/nm}$ or $D \approx 5 \text{ pixels/nm}$. Figure 7a–f shows the topographic view of the 3D excitation–emission spectra of samples A3, B4, A7, B8, A10, and B10, which correspond to the spectra in Figure 2 for the same samples.

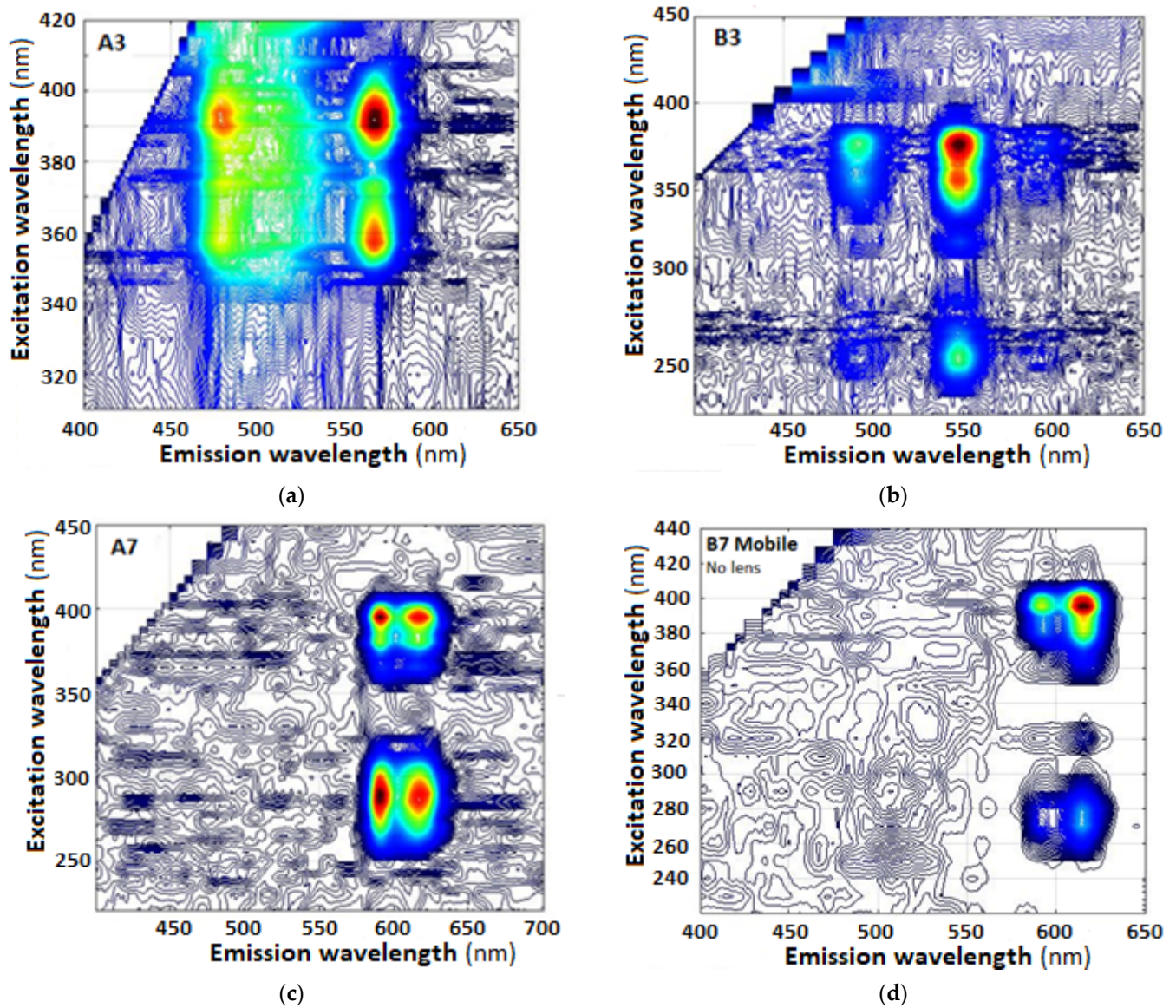


Figure 7. Cont.

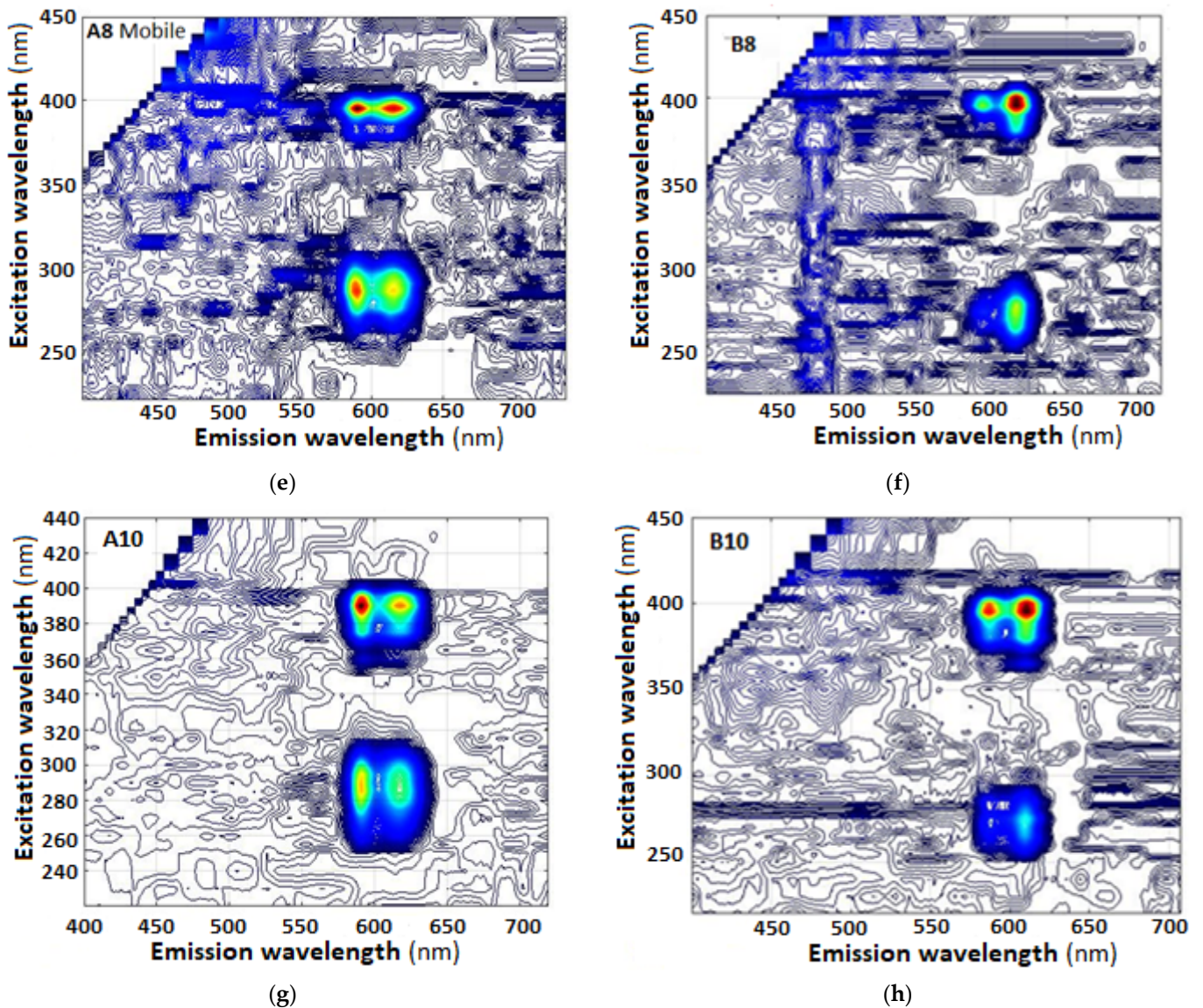


Figure 7. Topographic view of the excitation–emission fluorescence spectra of the two samples in Figure 3, taken by a smartphone: (a) A3; (b) B4; (c) A7; (d) B7; (e) A8; (f) B8; (g) A10 and (h) B10.

Figures 2 and 7 present the 3D spectra of (a) A3, (c) A7, (e) A8 and (g) A10 measured by the Ocean Optics spectrometer (OO) and of (b) B4, (d) B7, and (f) B8 and (h) B10 measured by the mobile phone (MP). A comparison between these 3D spectra allows for the enumeration of the following observations:

- (i) The smartphone accurately reproduces the narrow excitation–emission band within the 400 nm to 700 nm mobile phone sensitivity range and allows for the identification of the emission maxima of the samples in spite of the distortions mentioned in Section 4.1.
- (ii) The smartphone cuts off all spectral content above 700 nm, and above 650 nm, weak maxima are practically undetectable, which is a disadvantage. At the same time, it efficiently eliminates the spectra of the excitation light for wavelengths ≤ 395 nm and strongly reduces them up to 405 nm, which is an important advantage for fluorescence measurements.
- (iii) The smartphone modifies the proportions between neighboring peaks, which means that to identify the sample, the spectrum as measured by a smartphone must be known, especially in the case of ratiometric measurements.

- (iv) The smartphone efficiently cuts off the emission from the excitation sources in the UV range, as evidenced by Figure 6a,b, in which range the spectrometer may be saturated.

4.3. Measurements with a Lens

In this case, the setup is modified by adding an optional short-focal-length lens in combination with a 1 mm-diameter diaphragm. The unit is placed on the sample and collects light from a larger solid angle. Thus, the signal level is increased. However, due to the magnification, the size of the sample is enlarged and occupies a larger number of pixels on the screen of the mobile phone.

To illustrate the effect of the lens on the measured spectrum with an excitation wavelength close to the maximum excitation efficiency, which for the samples under study is in the range between 378 and 400 nm, we present in Figure 8 the fluorescence spectra of sample B7 as observed by the spectrometer and by a smartphone with and without a lens. We see that the visibility of the two peaks is the highest when measured by a spectrometer, lower when measured by the smartphone without lens, and worst when measured by a lens. The reason for the reduction in the visibility of the peaks is the poorer resolution, because unlike the spectrometer, no narrow slit is used to reduce the size of the image whose spectrum is being observed. A second reason is the saturation of the signal in the smartphone, as demonstrated in Figure 5d.

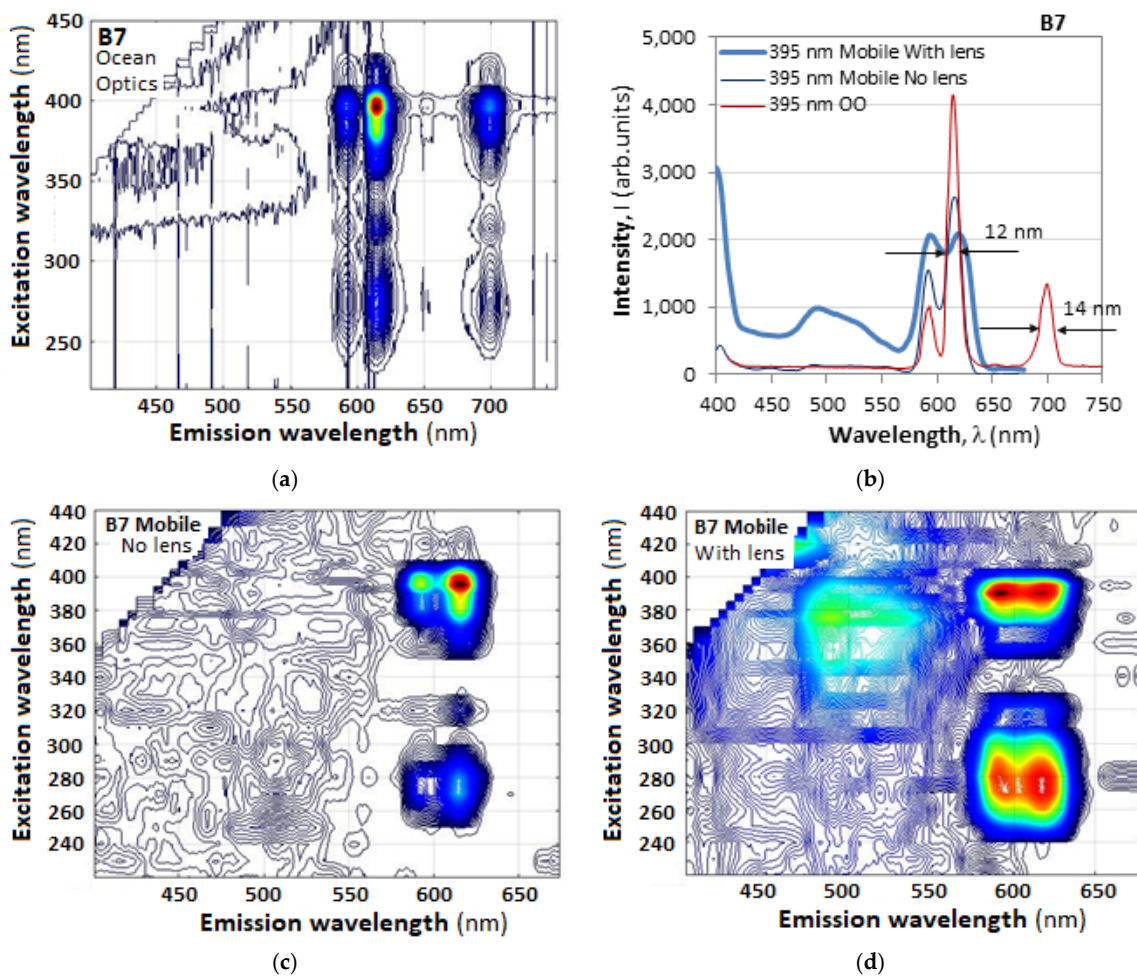


Figure 8. Illustration of the effect of using a magnifying lens for B7: (a) topographic view of the 3D excitation–emission spectra taken by a mobile with a lens; (b) comparison between the spectra of B7 excited at 395 nm taken by a spectrometer (Ocean Optics—OO) and a mobile phone with and without a lens. (c) sample B7 without lens and (d) sample B7 with lens.

When a lens is used, two effects are clearly observed. First, since the short-focal-length lens gathers light from a wider angle, the signal level is increased. Second, weak signals from the background and stray light become visible. The mobile phone, however, has a higher transmission in the green range as evidenced by Figure 4, which leads to the appearance of the weaker broader maxima around 500 nm as in Figures 8 and 9. Their presence is conditional on the existence of parasitic glares and background light and requires additional study.

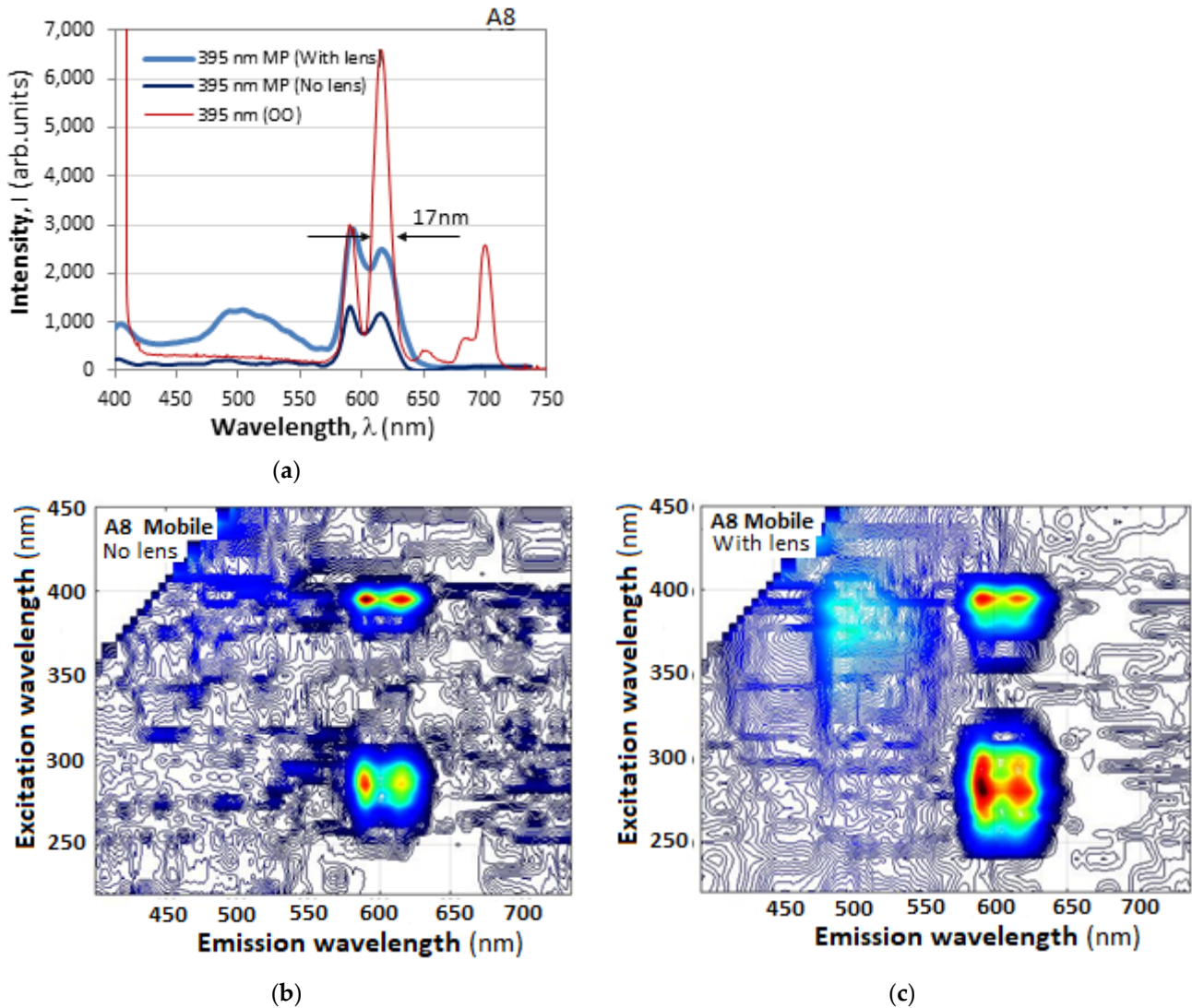


Figure 9. Illustration of the effect of using a magnifying lens for A8: (a) topographic view of the 3D excitation–emission spectra taken by a mobile phone with a lens; (b) comparison between the spectra of A8 excited at 395 nm taken by a spectrometer (OO) and a mobile phone with and without a lens; (c) same as (b) but with lens.

The same observations, to a different degree, are valid for samples B8 and B10 shown in Figures 10 and 11. In all cases, what is important for the purposes of this study is the possibility of clearly outlining and identifying the strong narrow excitation–emission spectra, which proves to be successful.

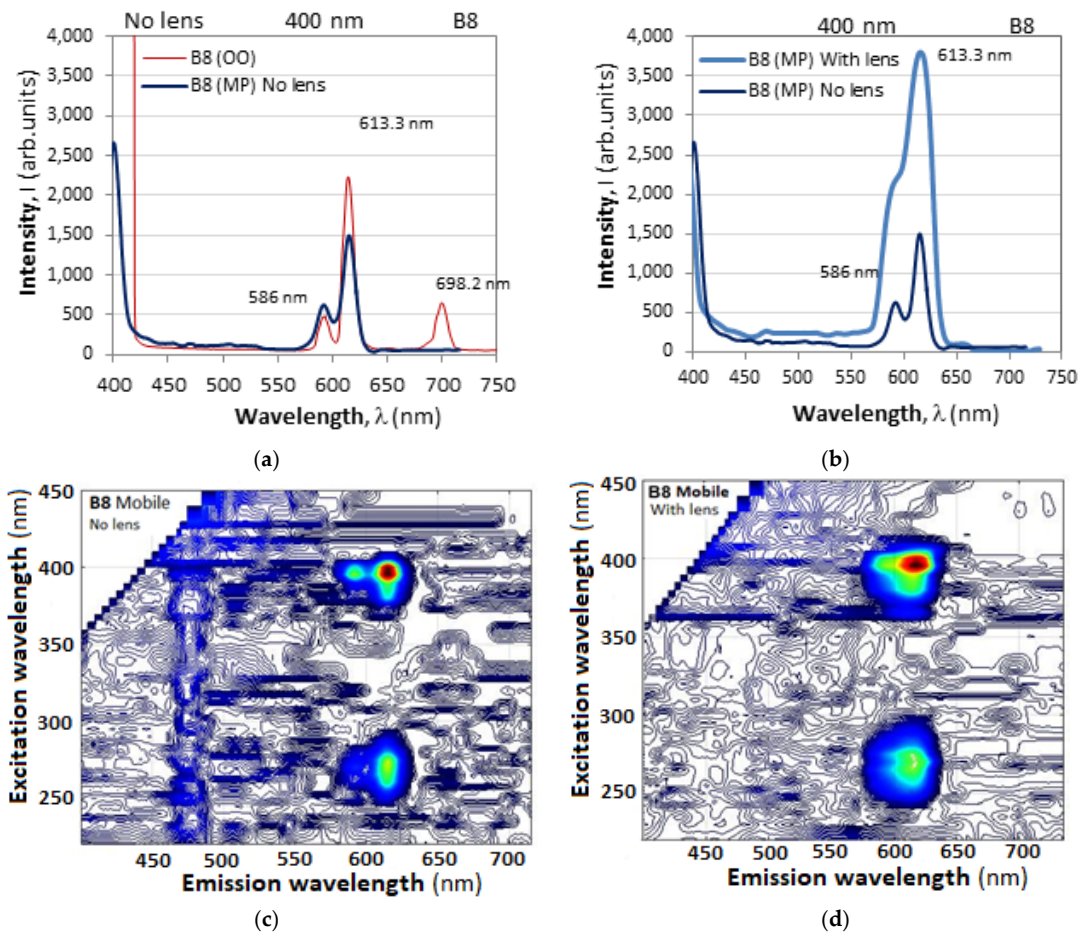


Figure 10. Illustration of spectral resolutions for B8: (a) Ocean Optics spectrometer spectrum vs. mobile phone spectrum without a lens; (b) mobile phone spectra with and without an additional lens; (c) topographic view of the 3D excitation–emission spectra of sample B8 taken by a mobile phone without lens; (d) same as (c) with a lens.

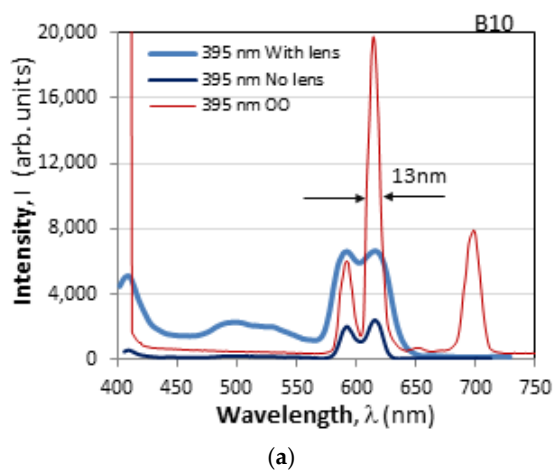


Figure 11. Cont.

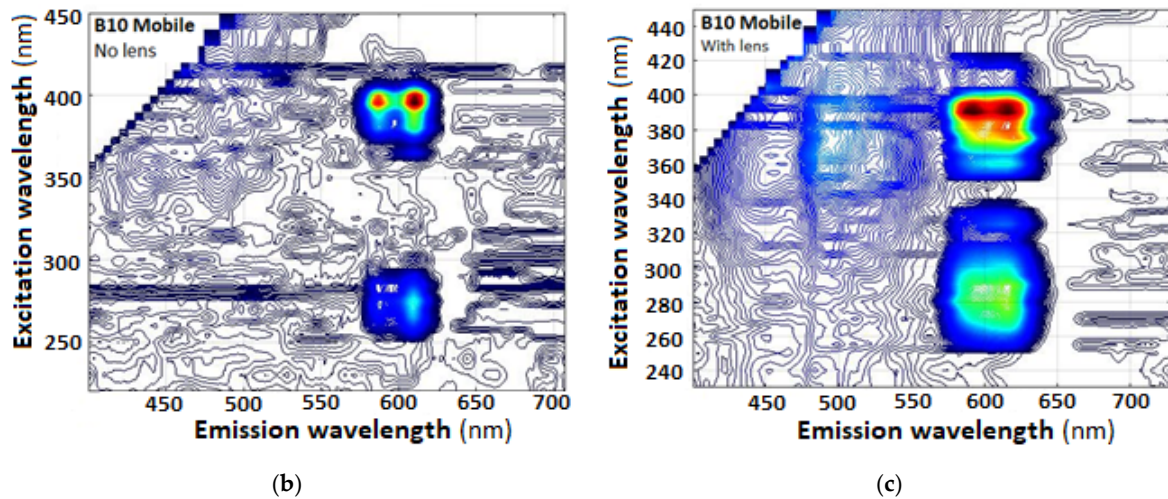


Figure 11. (a) Comparison between the spectra of B10 excited at 395 nm taken by a spectrometer (OO) and by a mobile phone with and without a lens. (b) A topographic view of the 3D excitation–emission spectra taken by a mobile phone without a lens; (c) same as (b) but with a lens.

In all cases, the RGB pixel filters strongly reduce the peak of the excitation light at wavelengths ≤ 400 nm, which is an important advantage. The effects of the additional magnification lens can be summarized as follows:

- (i) The lens increases the level of the signal at the expense of reduced visibility and resolution.
- (ii) The increased signal level may cause the appearance of spectral noise in the blue–green range because of background light and glares.

5. Measurements with LED Sources

For the majority of applications of borates with smartphone interrogation, the excitation source is an LED or a laser diode, rather than a monochromator. In this case, the possible excitation wavelengths are limited in number, and the excitation wavelength of maximum intensity may be different from that of maximum efficiency. This may be a serious problem, since the excitation bandwidth of high efficiency is of the order of the bandwidth of an LED, i.e., 15–20 nm. To compare the monochromator with LED excitation, we carry out measurements with UV LEDs whose maximum intensity wavelength is close to the maximum efficiency wavelength. Some of the results are presented in Figures 12–14.

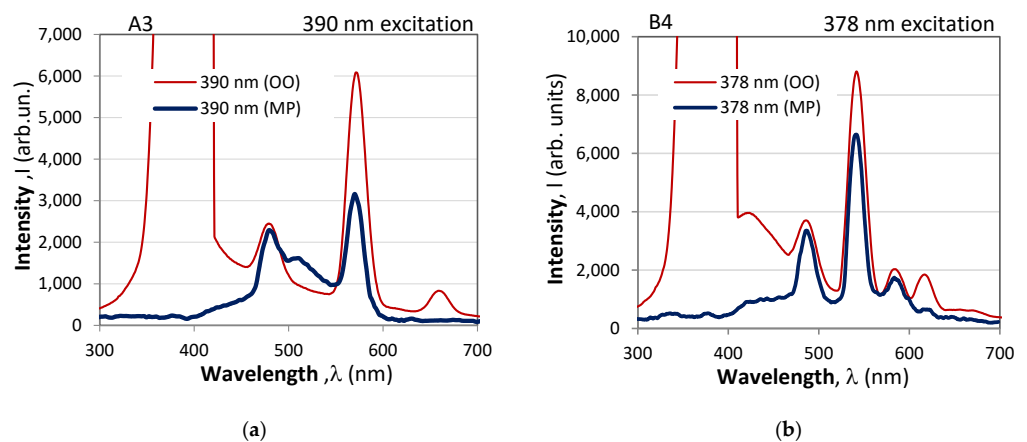
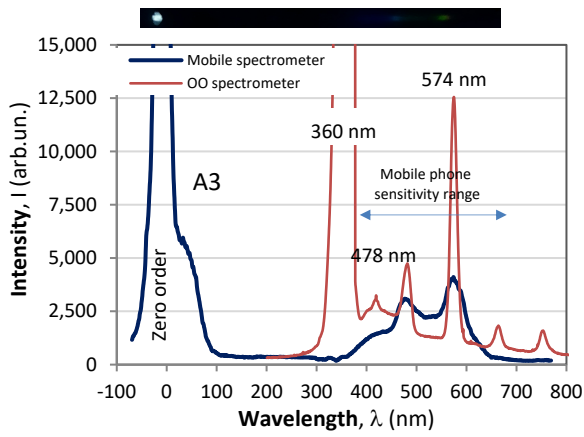
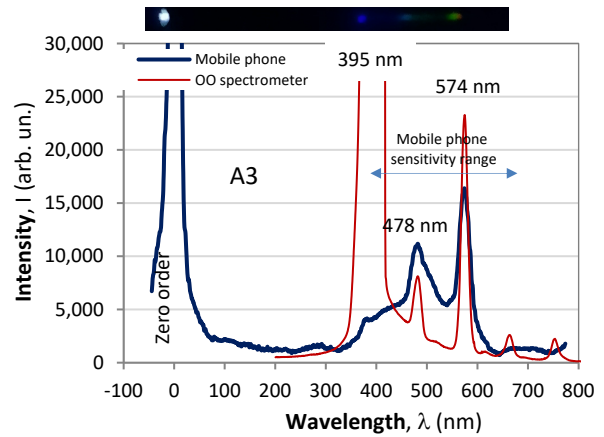


Figure 12. Comparison between the spectra of samples (a) A3 and (b) B4 measured by an Ocean Optics spectrometer and a smartphone at wavelengths of maximum excitation efficiency.

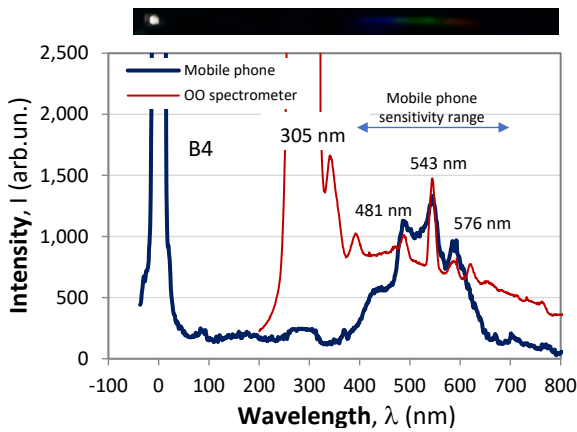


(a)

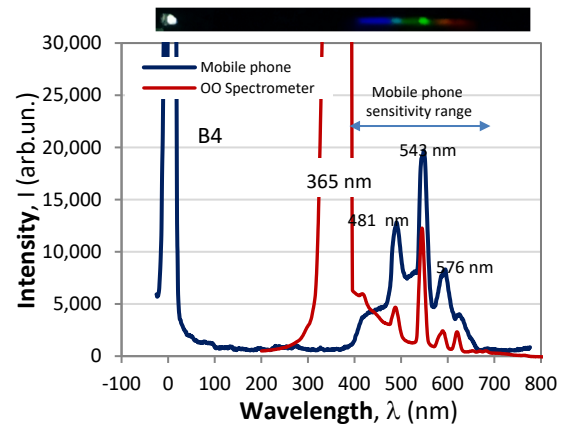


(b)

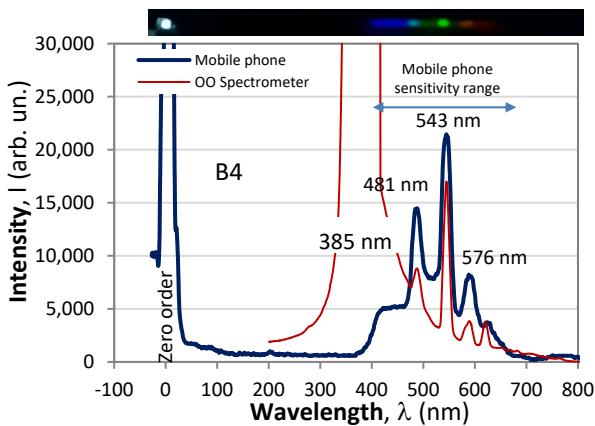
Figure 13. Comparison between the spectra measured by standard and mobile spectrometers for the A3 sample: (a) LED excitation at 360 nm; (b) LED excitation at 395 nm.



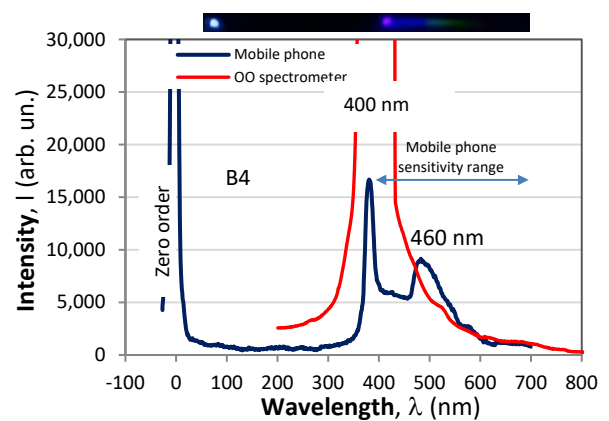
(a)



(b)



(c)



(d)

Figure 14. Comparison between the spectra measured by standard and mobile spectrometers for the S 62 SS sample: (a) LED excitation at 305 nm; (b) LED excitation at 365 nm; (c) LED excitation at 385 nm; (d) LED excitation at 400 nm.

The spectra at the same LED excitation measured by the spectrometer and the mobile phone are presented in the same graphs, which allows for the formulation of the following observations:

- (i) The mobile phone outlines the characteristic narrow-emission spectral peaks of the samples under study.
- (ii) The mobile phone very efficiently blocks the UV excitation light, and in the case when the excitation wavelength is close to the emission peak, the latter is still detectable (see Figure 14d).
- (iii) The mobile phone strongly attenuates all peaks above 670 nm.

6. Arrays of Fluorescent Markers

Since the smartphone efficiently blocks UV excitation and allows for the identification of the narrow-band spectral signatures of the different samples, we now investigate the possibility of discerning markers of these samples arranged in linear arrays so as to form specific patterns.

6.1. Basic Arrangement

Figure 15 presents the experimental arrangement to simultaneously illuminate a large number of samples. A glass cylinder is placed in front of the UV LED to form a thin line, which simultaneously excites up to 10 samples placed in holes of 1 mm in diameter in an opaque plate. Since the intensity of the light focused into a line is not uniformly distributed, we take the spectra of the samples in two groups of five.

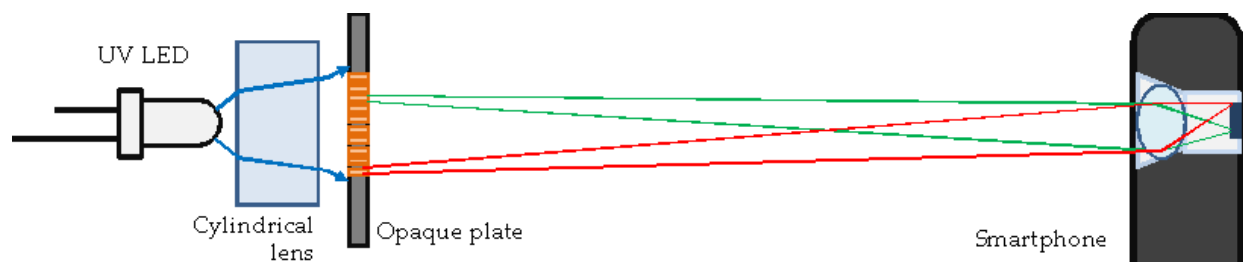


Figure 15. Experimental setup to simultaneously observe the spectra of fluorescent arrays.

6.2. Results and Comments

Using the arrangement in Figure 15, we perform a simultaneous observation of the spectra of 10 of the samples, namely A1, A2, A3, A7, A8, A10, B4, B5, B9, and B10, arranged in a column. Figure 16a–d shows the spectra under 365 nm, 375 nm, 385 nm, and 395 nm LED excitation. We note that when the excitation wavelength is varied, the observed spectral arrays are noticeably changed. The strongest signal is for the 385 nm and 395 nm excitations and the wings of the excitation wavelengths are more pronounced than at 365 nm and 375 nm. These spectra suggest that in the case of a two-level encoding scheme in which a “0” (black) is attributed to a signal below a given threshold and a “1” (white) to a signal above the threshold, the four colored patterns in Figure 16 would appear as different black-and-white 2D spatial patterns.

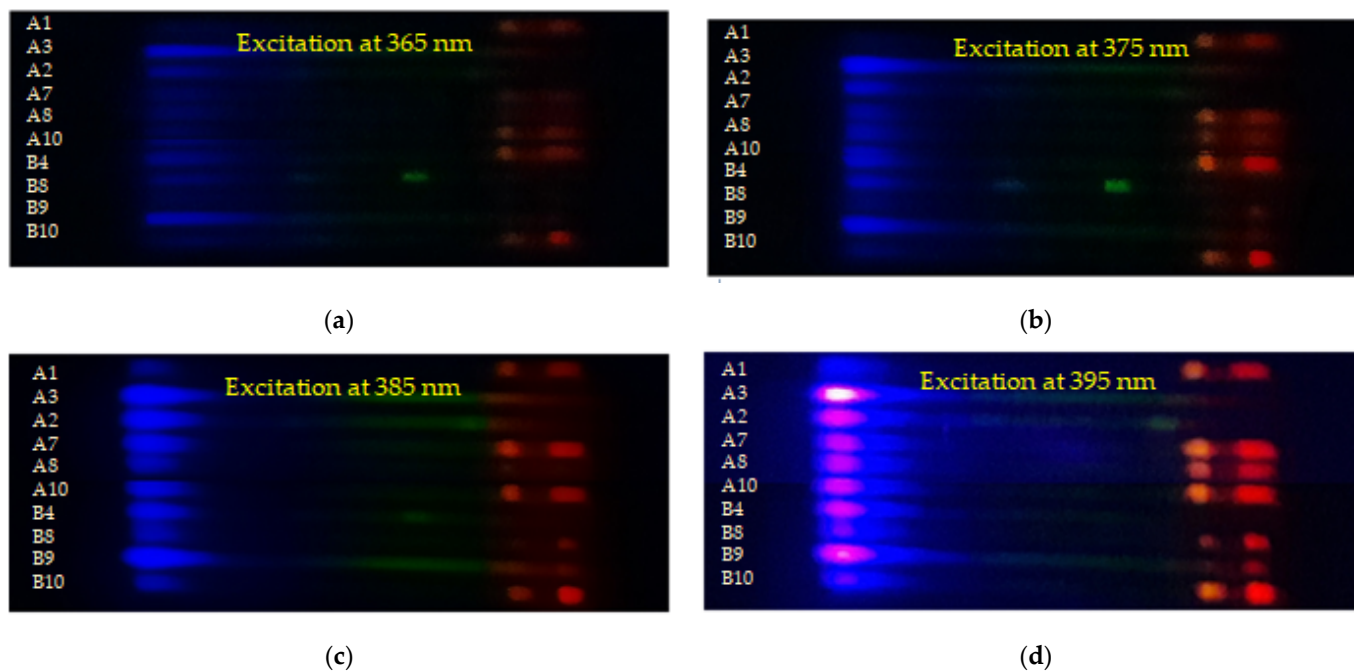


Figure 16. Experimental setup to simultaneously observe the spectra of fluorescent arrays.

The research performed and the results obtained outline the need for some further research in view of the possible applications related to luminescent markers using remote sensing and interrogation. In the first place, the deformations of the spectral response compared to those of spectrometers must be studied for a variety of makes of smartphones and for different levels of signals. Second, a more detailed study on the use of additional lenses to augment signal level must be performed, as well as on the effect of the internal magnification of the smartphone camera on the measured spectrum. Third, the spectral responses in the case of arrays of fluorescent materials, and last, the improvement of the synthesis technology to obtain more efficient luminescence with more repeatable characteristics must all be studied.

7. Conclusions

The experiments and the analysis performed allow for the formulation of the following conclusions:

- C1. The synthesized rare-earth-doped lanthanum and aluminum borates are characterized by spectra that are as narrow as $\Delta\lambda' = 15 \text{ nm}$ for the excitation and $\Delta\lambda = 12 \text{ nm}$ FWHM for the emission bandwidths, which are comparable to the emission band when LEDs are used as excitation sources.
- C2. The particular peaks of maximum excitation–emission wavelengths depend on the particular rare earth dopants and their combinations, and in the general case, lanthanum borates demonstrate a higher luminescence intensity compared to the aluminum borates for the orange–red emission peaks (586 nm/613 nm) and comparable intensities to the green peak (543 nm).
- C3. Because the maximum efficiency excitation band $\Delta\lambda'$ is practically the same as the LED emission bandwidth, the studied La and Al borates are particularly appropriate for UV LED excitation in the 375 nm–395 nm range to serve as selective fluorescent markers for a number of applications.
- C4. Smartphones equipped with a low-cost transmission diffraction grating can efficiently be used for the contactless detection of the synthesized materials.
- C5. Because of their RGB filter characteristics, smartphones efficiently attenuate the excitation outside the visible range and are therefore useful in the case when excitation in the infrared is based on upconversion [26].

- C6. Compared to spectrometers, smartphones exhibit a rather non-uniform spectral sensitivity curve featuring several maxima as well as a power-law-diminishing intensity ratio.
- C7. Smartphones allow for the plotting of 3D excitation–emission spectra and accurately identify the individual excitation–emission peaks of the particular samples. However, as the spectral sensitivity of the smartphone is determined by the transmission spectra of its RGB filters and the diminishing smartphone-to-spectrometer intensity ratio, the relative intensities of the different peaks may differ from those measured by a standard spectrometer.
- C8. The use of an additional short-focal-length lens in combination with the smartphone increases the intensity of the detected signal since more light is gathered, but on the other hand, it reduces the resolution and contrast in the detection of closely spaced peaks. It may also create some spectral noise in the green part of the spectrum.
- C9. Unlike the standard spectrometer, the smartphone allows for the simultaneous detection of the spectra of arrays of the studied fluorescent markers, of which the spatial distribution will appear different depending on the particular excitation.

Author Contributions: Conceptualization, K.H., I.P.K. and T.A.E.; methodology, K.H. and T.A.E.; software, D.B.; validation, I.P.K. and T.A.E.; formal analysis, T.A.E.; investigation, K.H., S.F. and T.A.E.; resources, K.H. and I.P.K.; data curation, D.B.; writing—original draft preparation, K.H. and T.A.E.; writing—review and editing, I.P.K.; visualization, D.B. and S.F.; supervision, I.P.K. and T.A.E.; project administration, I.P.K.; funding acquisition, T.A.E. All authors have read and agreed to the published version of the manuscript.

Funding: This research was funded by NSERC (Natural Sciences and Engineering Research Council) Discovery Grant, Canada.

Data Availability Statement: The raw data supporting the conclusions of this article will be made available by the authors on request.

Conflicts of Interest: The authors declare no conflicts of interest.

References

1. Abacı, Ö.C.H.; Mete, E.; Esenturk, O.; Yılmaz, A. Tunable optical properties and DFT calculations of RE³⁺ codoped LaBO₃ phosphors. *Opt. Mater.* **2019**, *98*, 109487. [[CrossRef](#)]
2. Cornejo, C.R. Luminescence in Rare Earth Ion-Doped Oxide Compounds (Ch.3). In *Luminescence—An Outlook on the Phenomena and Their Applications*; Thirumalai, J., Ed.; InTech: New Delhi, India, 2016; pp. 33–63.
3. Richardson, F.S. Terbium (III) and europium (III) ions as luminescent probes and stains for biomolecular systems. *Chem. Rev.* **1982**, *82*, 541–552. [[CrossRef](#)]
4. Nagpure, P.A.; Bajaj, N.S.; Sonekar, R.P.; Omanwar, S.K. Synthesis and luminescence studies of novel rare earth activated lanthanum pentaborate. *Indian J. Pure Appl. Phys.* **2011**, *49*, 799–802.
5. Ike, P.O.; Folley, D.E.; Agwu, K.K.; Chithambo, M.L.; Chikwembani, S.; Ezema, F.I. Influence of dysprosium doping on the structural, thermoluminescence and optical properties of lithium aluminium borate. *J. Lumin.* **2021**, *233*, 117932. [[CrossRef](#)]
6. Ike, P.O.; Nwanya, A.C.; Agwu, K.K.; Ezema, F.I. Optical and thermoluminescence response of rare earth activated aluminium borate crystals. *Opt. Mater.* **2022**, *127*, 112263. [[CrossRef](#)]
7. Fu, L.; Zhao, X.; Meng, Z.; Zhang, J.; Chu, G. Characterization and luminescent properties of lanthanum borate prepared by solution combustion method. *Mater. Sci. Eng. B* **2023**, *291*, 116362. [[CrossRef](#)]
8. Zhu, Q.; Fan, Z.; Li, S.; Li, J.-G. Implanting bismuth in color-tunable emitting microspheres of (Y, Tb, Eu)BO₃ to generate excitation-dependent and greatly enhanced luminescence for anti-counterfeiting applications. *J. Asian Ceram. Soc.* **2020**, *8*, 542–552. [[CrossRef](#)]
9. Lee, J.K.; Hua, Y.; Yu, J.S. High-quality reddish-orange-emitting Sr₆Y₂Al₄O₁₅:Eu³⁺ phosphors for solid-state lighting and anti-counterfeiting applications. *Ceram. Int.* **2024**, *50*, 484–494. [[CrossRef](#)]
10. Ingle, J.T.; Sonekar, R.P.; Omanwar, S.K. Combustion synthesis and superior photo-luminescence from rare earth doped (Eu, Tb) lanthanum borates phosphors for display. *J. Mater. Sci. Mater. Electron.* **2016**, *27*, 10735–10741. [[CrossRef](#)]
11. Paterson, A.S.; Raja, B.; Mandadi, V.; Townsend, B.; Lee, M.; Buell, A.; Vu, B.; Brigoche, J.; Willson, R.C. A low-cost smartphone-based platform for highly sensitive point-of-care testing with persistent luminescent phosphors. *Lab Chip* **2017**, *17*, 1051–1059. [[CrossRef](#)]
12. Ramalho, J.F.C.B.; António, L.C.F.; Correia, S.F.H.; Fu, L.S.; Pinho, A.S.; Brites, C.D.S.; Carlos, L.D.; André, P.S.; Ferreira, R.A.S. Luminescent QR codes for smart labelling and sensing. *Opt. Laser Technol.* **2018**, *101*, 304–311. [[CrossRef](#)]

13. Shahvar, A.; Shamsaei, D.; Saraji, M. A portable smartphone-based colorimetric sensor for rapid determination of water content in ethanol. *Measurement* **2020**, *150*, 107068. [[CrossRef](#)]
14. Xu, J.; Zhang, Y.; Li, Y.; Zhao, D.; Zhang, L.; Bi, N.; Gou, J.; Zhao, T.; Jia, L. Multifunctional dual-channel fluorescent nanoprobe for visual fluorescence detection of pathogenic bacteria and excessive antibiotics in food safety. *J. Lumin.* **2024**, *266*, 120303. [[CrossRef](#)]
15. Tominaga, S.; Nishi, S.; Ohtera, R. Measurement and Estimation of Spectral Sensitivity Functions for Mobile Phone Cameras. *Sensors* **2021**, *21*, 4985. [[CrossRef](#)]
16. Piłuła, E.; Koba, M.; Smietana, M. Which smartphone for a smartphone-based spectrometer? *Opt. Laser Technol.* **2021**, *140*, 107067. [[CrossRef](#)]
17. Swapna, K.; Mahamuda, S.; Rao, A.S.; Jayasimhadri, M.; Shakya, S.; Prakash, G.V. Tb³⁺ doped Zinc Alumino Bismuth Borate glasses for green emitting luminescent devices. *J. Lumin.* **2014**, *156*, 180–187. [[CrossRef](#)]
18. Murthy, K.V.R.; Sai Prasad, A.S.; Rao, M.R. Luminescence Characteristics of Eu and Tb Doped YGdBO₃ Phosphor. *Phys. Procedia* **2012**, *29*, 70–75. [[CrossRef](#)]
19. Pisarski, W.A.; Pisarska, J.; Dominiak-Dzik, G.; Mączka, M.; Ryba-Romanowski, W. Compositional-dependent lead borate based glasses doped with Eu³⁺ ions: Synthesis and spectroscopic properties. *J. Phys. Chem. Solids* **2006**, *67*, 2452–2457. [[CrossRef](#)]
20. Pisarska, J.; Kos, A.; Sottys, M.; Żur, L.; Pisarski, W.A. Energy transfer from Tb³⁺ to Eu³⁺ in lead borate glass. *J. Non-Cryst. Solids* **2014**, *388*, 1–5. [[CrossRef](#)]
21. Van Do, P.; Ngoc, T.; Ca, N.X.; Thanh, L.D.; Thanh Nga, P.T.; Chung Thuy, T.T.; Van Nghia, N. Study of spectroscopy of Eu³⁺ and energy transfer from Ce³⁺ to Eu³⁺ in sodium-zinc-lead-borate glass. *J. Lumin.* **2020**, *229*, 117660.
22. Ebendorff-Heidepriem, H.; Ehrhart, D. Formation and UV absorption of cerium, europium and terbium ions in different valencies in glasses. *Opt. Mater.* **2000**, *15*, 7–25. [[CrossRef](#)]
23. Sankara, R.; Subba Rao, G.V. Eu³⁺ Luminescence, Ce⁴⁺ → Eu³⁺ Energy Transfer, and White-Red Light Generation in Sr₂CeO₄. *J. Electrochem. Soc.* **2000**, *147*, 2773. [[CrossRef](#)]
24. Wantana, N.; Kaewnuam, E.; Chanlek, N.; Kim, H.J.; Kaewkhao, J. Influence of Gd³⁺ on structural and luminescence properties of new Eu³⁺-doped borate glass for photonics material. *Radiat. Phys. Chem.* **2023**, *207*, 110812. [[CrossRef](#)]
25. Hristova, K.; Kostova, I.; Eftimov, T.; Tonchev, D. Synthesis and Luminescent Characteristics of Yttrium, Aluminium and Lanthanum Borates Doped with Europium Ions (Eu³⁺). *Bulg. Chem. Commun.* **2024**. *accepted for publication*.
26. Zhu, D.; Guo, K.; Yao, J.; Duan, B.; Wu, Y.; Li, Y.; Wang, F.; Liu, T.; Hu, J. The single near-infrared upconversion luminescence of a novel KYb (MoO₄)₂: Er³⁺ phosphor for the temperature sensing. *J. Mol. Struct.* **2024**, *1310*, 138304. [[CrossRef](#)]

Disclaimer/Publisher's Note: The statements, opinions and data contained in all publications are solely those of the individual author(s) and contributor(s) and not of MDPI and/or the editor(s). MDPI and/or the editor(s) disclaim responsibility for any injury to people or property resulting from any ideas, methods, instructions or products referred to in the content.